JOURNAL OF GEOPHYSICAL RESEARCH, VOL. 113, A05205, doi:10.1029/2007JA012609, 2008

A magnetic null geometry reconstructed from Cluster spacecraft observations

J.-S. He,[1] C.-Y. Tu,[1] H. Tian,[1] C.-J. Xiao,[2] X.-G. Wang,[3] Z.-Y. Pu,[1] Z.-W. Ma,[4] M. W. Dunlop,[5] H. Zhao,[2] G.-P. Zhou,[2] J.-X. Wang,[2] S.-Y. Fu,[1] Z.-X. Liu,[6] Q.-G. Zong,[1,7] K.-H. Glassmeier,[8] H. Reme,[9] I. Dandouras,[9] and C. P. Escoubet[10]

Received 26 June 2007; revised 3 December 2007; accepted 22 January 2008; published 6 May 2008.

[1] This paper reports for the first time the identification of a magnetic structure around a magnetic null in a magnetic reconnection region in the magnetotail. Magnetic reconnection is one of the fundamental processes in astrophysical and solar-terrestrial plasmas. Though the concept of reconnection has been studied for many years, the process that really occurs has not been fully revealed by direct measurements. In particular, the lack of a description of three-dimensional (3-D) reconnecting magnetic field from observations makes the task more difficult. The Cluster spacecraft array provide an opportunity to reconstruct the 3-D magnetic reconnection structure based on magnetic field vectors simultaneously measured at four positions. The identification of this structure comes from a new method of analysis of in situ measurements proposed here. Applying a fitting model of 10 spherical harmonic functions and a Harris current sheet function, plus a constant field, we reconstruct a 3-D magnetic field configuration around the magnetic null in an reconnection event observed by Cluster in the geo-magnetotail.

Citation: He, J.-S., et al. (2008), A magnetic null geometry reconstructed from Cluster spacecraft observations, *J. Geophys. Res.*, *113*, A05205, doi:10.1029/2007JA012609.

1. Introduction

[2] Magnetic reconnection is an important physical process which changes the topology of magnetic fields in magnetized plasmas, converts magnetic energy to plasma dynamic energy and accelerates particles. The concept of magnetic reconnection helps to explain and accounts for most of the energy release and transfer processes observed in solar-terrestrial plasmas.

[3] Theoretical studies of magnetic reconnection have made great progress [e.g., *Priest and Forbes*, 2000; *Birn and Priest*, 2007] since the initial reconnection models were proposed [e.g., *Sweet*, 1958; *Parker*, 1957]. Nevertheless, the underlying physical process has not yet been completely discovered by direct measurements. A major difficulty is how to identify the complicated magnetic configurations and plasma flow patterns predicted by the theory. In two-dimensional (2-D) reconnection, for example, various field and plasma configuration features such as current sheets, slow shocks, Hall quadruple components, and a guide field have been thoroughly studied, and their properties are more or less well understood [e.g., *Petschek*, 1964; *Nagai et al.*, 2001; *Birn et al.*, 2001; *Pritchett and Coroniti*, 2004; *Ricci et al.*, 2004]. For 3-D (three-dimensional) reconnection, however, complicated magnetic field topologies consisting of null points, spines, fans, and separators have also been implied, and various reconnection models such as spine reconnection, fan reconnection, and separator reconnection have been suggested [e.g., *Greene*, 1988; *Priest and Forbes*, 1989; *Priest and Titov*, 1996; *Parnell et al.*, 1996; *Priest and Demoulin*, 1995; *Büchner*, 1999].

[4] In fact, to identify a specific 3-D reconnection model from observations, it is necessary to describe both the flow pattern and the magnetic field configuration in a small scale region around the reconnection site. Such an attempt has been made for decades in laboratory experiments and through solar atmosphere and magnetosphere observations. In laboratory plasmas, magnetic field diagnostic is still a great challenge to experimentalists [e.g., *Ding et al.*, 2004], and therefore it is difficult to properly construct the related 3-D current density distribution [e.g., *Priest and Forbes*, 2000]. In the solar atmosphere, global 2-D and 3-D reconnection configurations can be roughly approximated from solar images of certain radiation or scattering lines [e.g., *Lin*

[1]School of Earth and Space Sciences, Peking University, Beijing, China.
[2]National Astronomical Observatories, Chinese Academy of Sciences, Beijing, China.
[3]School of Physics, Peking University, Beijing, China.
[4]Institute for Fusion Theory and Simulation, Zhejiang University, Hangzhou, China.
[5]Space Sciences Division, SSTD, Rutherford Appleton Laboratory, Chilton, Oxfordshire, UK.
[6]CSSAR, Chinese Academy of Sciences, Beijing, China.
[7]Center for Atmospheric Research, University of Massachusetts Lowell, Lowell, Massachusettes, USA.
[8]IGEP, Technische Universität Braunschweig, Braunschweig, Germany.
[9]Centre d'Etude Spatiale des Rayonnements, Toulouse, France.
[10]ESA/ESTEC, Noordwijk, Netherlands.

0148-0227/08/2007JA012609$09.00

et al., 2005; *Filippov*, 1999] or derived from the surface magnetic field distribution of the photosphere based on either force-free or potential-field assumptions [e.g., *Aulanier et al.*, 2000; *Fletcher et al.*, 2001; *Zhao et al.*, 2005]. However, it is hard to obtain a related flow pattern from either method.

[5] In the Earth's magnetosphere, 3-D reconnection characteristics at the dayside terrestrial magnetopause have been investigated through resistive MHD simulation, and separator reconnection has been predicted under generic northward interplanetary magnetic field conditions [*Dorelli et al.*, 2007]. Satellite in situ measurements can be used to check the theoretical predictions and simulation results. Satellite measurements have detected, in particular, 2-D reconnection features, such as the flow reversal, quadruple magnetic field associated with the Hall current, whistler and lower hybrid waves near or in the reconnection region in a number of reconnection events [e.g., *Phan et al.*, 2000; *Øieroset et al.*, 2001; *Deng and Matsumoto*, 2001; *Frey et al.*, 2003; *Henderson et al.*, 2006; *Vaivads et al.*, 2004]. However, 3-D reconnection features have rarely been observed, and in particular continuous magnetic field distributions derived from observations have not been reported. The lack of a real-time description of 3-D field configurations around the reconnection site weakens the preciseness and solidity of the related reconnection models and analysis.

[6] The Cluster mission [*Escoubet et al.*, 1997] is designed to perform 4-point measurements in geospace. The main scientific objective of the mission is to study small-scale 3-D structures in the Earth's magnetosphere and near-Earth solar wind. Recently the existence of a 3-D magnetic null point at a reconnection site in the magnetotail was reported based on the method using Poincaré index and the measurements taken by the four separately positioned Cluster spacecraft [*Xiao et al.*, 2006]. The determination of a magnetic null is the first step in exploring the 3-D reconnection feature from in situ measurements. The Poincaré index method, however, requires the closed surface to be sampled surrounding the null and a large number of field samples on the surface. The Cluster can sample only four field vectors at the same time. The magnitudes of the Cluster magnetic field surrounding the null reported by [*Xiao et al.*, 2006] total about 20 nT, which is a rather large value for the field in the magnetotail. Therefore the closed tetrahedron surface made by the four cluster spacecraft does not lie close to the null. Furthermore, the 3-D field configuration near the reconnection site has not yet been modeled.

[7] We propose here a new method to reconstruct a local magnetic field configuration based on the four magnetic vectors observed by the Cluster constellation. By applying this method to the in situ measurements, we reconstruct the magnetic field configuration around a reconnection site. With this fitted magnetic field we can calculate the Poincaré index with a closed surface very near to the null, rather than with the peripheral tetrahedron made by the four Cluster spacecraft. The data were taken while Cluster was in a magnetic reconnection region in the magnetotail on 15 September 2001. We find for the first time from in situ measurements, a magnetic structure around a 3-D null. We believe the fitting method and the reconstructed field structure cast new lights on nature of 3-D magnetic reconnection.

2. Method Description

[8] In order to fit the recorded 4 vectors with 12 magnetic field components simultaneously measured by the Cluster satellites, we design a fitting model, based on a summation of 12 functions, which includes ten spherical harmonic functions and a function taken from the Harris current sheet model [*Harris*, 1962], together with a constant background field. We adopt the spherical harmonic functions as part of the fitting model for their convenience of describing a potential field. Considering the special feature of magnetic field configuration in the magnetotail, we add the Harris current sheet function with a constant background field to the fitting function. Such a fitting can be expressed as

$$\begin{pmatrix} B_r \\ B_\theta \\ B_\phi \end{pmatrix} = \begin{pmatrix} \widetilde{B_r} \\ \widetilde{B_\theta} \\ \widetilde{B_\phi} \end{pmatrix} + T_{xyz\to r\theta\phi} \cdot \begin{pmatrix} B_0 \tanh\left(\dfrac{z-z_0}{L_z}\right) + B_1 \\ 0 \\ 0 \end{pmatrix}, \quad (1)$$

where $(B_r\ B_\theta\ B_\varphi)$ represent 3 magnetic field components at a spatial position $(r\ \theta\ \varphi)$ in a spherical coordinate system with its origin at the center of the Earth. The first term on the right-hand side (RHS) of equation (1), ($\widetilde{B_r}$ and $\widetilde{B_\theta}$ and $\widetilde{B_\varphi}$), is the contribution from the spherical harmonic series describing a potential field, as shown below in equation (2). The transform matrix $T_{xyz\to r\theta\phi}$ converts a vector field from the GSM to a geocentric spherical coordinate system. The magnetic field in the Harris current model plus a constant background field is in the x-direction as shown in equation (1). Expression for $(\widetilde{B_r}\ \widetilde{B_\theta}\ \widetilde{B_\varphi})$ reads

$$\begin{pmatrix} \widetilde{B_r} \\ \widetilde{B_\theta} \\ \widetilde{B_\varphi} \end{pmatrix} = \begin{pmatrix} \sum\limits_n \sum\limits_m -(n+1)\left(\dfrac{R_e}{r}\right)^{n+2} \cdot \left(q_n^m \cos(m\varphi) + h_n^m \sin(m\varphi)\right) \cdot P_n^m(\cos\theta) \\ \dfrac{R_e}{r} \sum\limits_n \sum\limits_m \left(\dfrac{R_e}{r}\right)^{n+1} \cdot \left(q_n^m \cos(m\varphi) + h_n^m \sin(m\varphi)\right) \cdot (-\sin\theta) \cdot \dfrac{\partial}{\partial\theta}\left(P_n^m(\cos\theta)\right) \\ \dfrac{R_e}{r\sin\theta} \sum\limits_n \sum\limits_m \left(\dfrac{R_e}{r}\right)^{n+1} \cdot \left(q_n^m \cdot (-m) \cdot \sin(m\varphi) + h_n^m \cdot m \cdot \cos(m\varphi)\right) \cdot P_n^m(\cos\theta) \end{pmatrix}, \quad (2)$$

where q_n^m and h_n^m are the coefficients in the spherical harmonic series, and P_n^m is the associated Legendre function of degree n and order m, with $[n, m] = \{[1,1], [2,1], [\{2,2\}], [3,1], [3,2]\}$. The second term on the RHS of equation (1) is designed specifically to represent the magnetotail environment. When the Cluster constellation is in the lobe where the magnetic field is mainly earthward or tailward, the background field B_1 dominates over the Harris magnetic field configuration. Conversely, when Cluster is near the current sheet, the local magnetic field configuration may be represented mainly by the Harris configuration. Since both

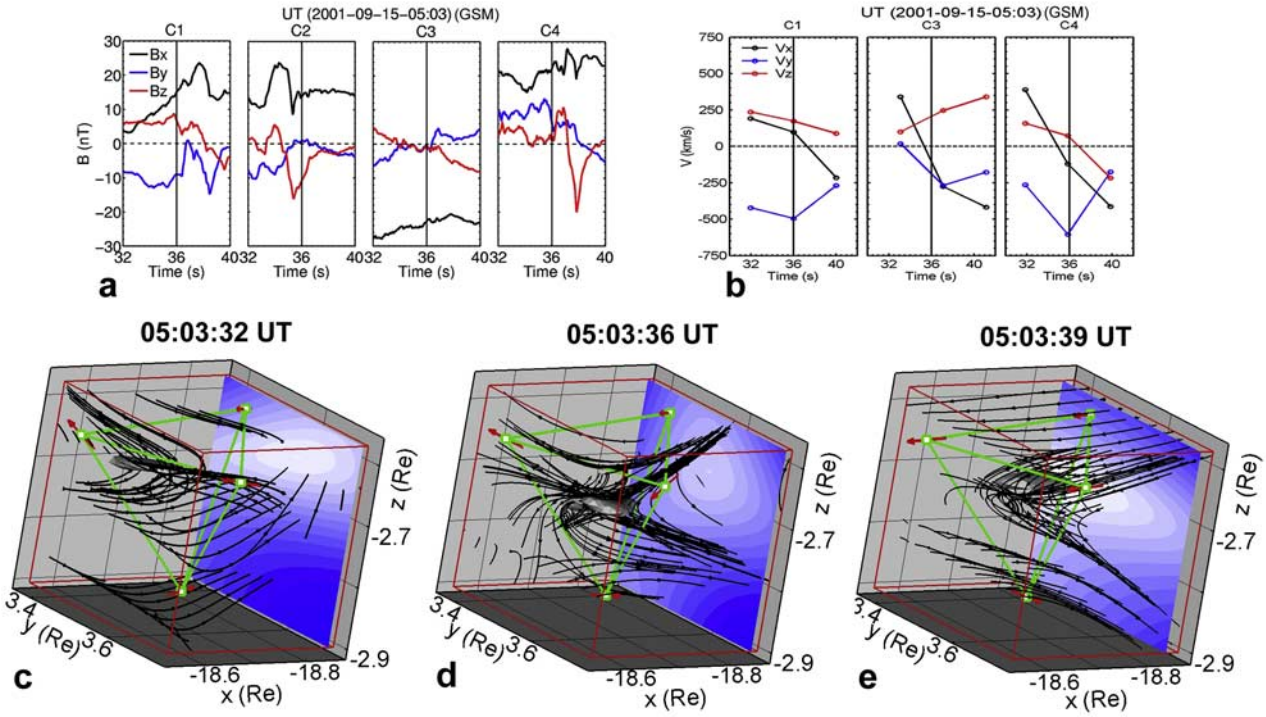

Figure 1. An event of reconnection region crossing in the magnetotail by Cluster. (a) Temporal variations of magnetic field components (B_x, B_y, B_z) in GSM with a 0.04 s resolution in the interval of 05:03:32-05:03:40 UT as measured by FGM on board C1, C2, C3 and C4 (from left to right). B_x, B_y and B_z are plotted in black, blue and red respectively. (b) Plasma velocity components (V_x, V_y, V_z) in GSM respectively in black, blue and red as measured by CIS on board C1, C3 and C4 (from left to right). (c-e) Reconstructed magnetic field structures in the GSM coordinates at 05:03:32, 05:03:36 and 05:03:39 UT based on measurements averaged over 1s. Magnetic field lines are represented with black lines and Cluster constellation tetrahedrons are marked in green. Four red arrows denote the local magnetic field directions. The contour projections on the right sides show the magnitude of B, from small to large as colored from white to blue.

the sum of the Legendre polynominals and the Harris current sheet satisfy $\nabla \cdot \vec{B} = 0$, the fitted field is automatically solenoidal.

[9] Two parameters for the Harris sheet configuration, L_z and z_0, are assumed in the following manner. In the case studied, the characteristic half thickness of the Harris current sheet, L_z, is taken as 920 km. For the purpose of estimating L_z, we take a set of data $\{z_3, B_{x3}, z_4, B_{x4}\}$ in a period from 05:03:20 to 05:03:42 to fit the formula $z_3 - z_4 = L_z\ [\tanh^{-1}\ (B_{x3}/B_0) - \tanh^{-1}\ (B_{x4}/B_0)]$, where z_3, z_4 are z coordinates in GSM of the Cluster C3 and C4 and B_{x3}, B_{x4} are x components of C3 and C4 respectively. It is found that L_z is about 920 km if B_0 lobe magnetic field is given as 33 nT which is a typical value of magnetic field in the geo-magnetotail lobe. This thickness scale is about twice as large as the typical ion inertial length of geomagnetotail. The other parameter z_0 is determined as follows. We first use a set of fitting functions expressed with a summation of 12 spherical harmonic functions to fit the magnetic field with the same observation data. Degree n and order m for these spherical harmonic functions are taken as: $[n, m] = \{[1,1], [2,1], [2,2], [3,1], [3,2], [3,3]\}$. In this test fitting, the minimum magnetic field strength can be found at (x_0, y_0, z_0), where z_0 is the parameter to be taken. In our calculation, the minimum magnetic field strength is about 0.41 nT in the potential field obtained by fitting four magnetic field vectors measured at 05:03:36. The GSM position of this minimum magnetic field is at (−18.67, 3.62, −2.68) Re. After L_z and z_0 are given, the 12 parameters including five q_n^m, five h_n^m, B_0, and B_1 can be determined with the 12 observed magnetic field components by exactly solving equation (1). The magnetic null is found at (−18.58, 3.64,−2.68) Re.

3. Data Analysis

[10] We use the fitting method described above to reconstruct the magnetic field near the magnetic reconnection site observed by Cluster in the magnetotail on 15 September 2001 from 05:03:32 to 05:03:40 UT. This magnetic reconnection event has already been studied elsewhere [e.g., *Xiao et al.*, 2006, 2007], and an isolated null point has been identified in the reconnection region around 05:03:36 UT, by using topological analysis of the magnetic field [*Xiao et al.*, 2006].

[11] Magnetic field data measured by the FGM on board Cluster [*Balogh et al.*, 1997] in the time interval from 05:03:32 to 05:03:40 UT are used with 0.04 s resolution

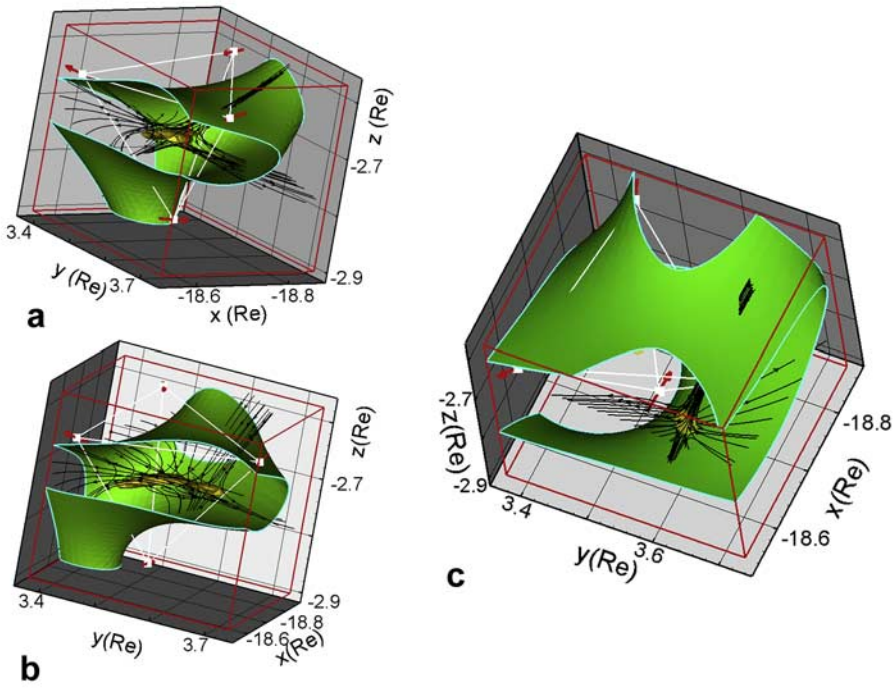

Figure 2. Magnetic structure reconstructed at 05:03:36 UT with a 1 s resolution viewed from different angles. (a) Appeared as an X-type topology viewed in the diagonal direction in the x-y plane. The green surface is with B = 16 nT, and the yellow surface is with B = 2.5 nT. The tetrahedron formed by Cluster constellation is denoted in white lines and dots, with 4 red arrows indicating the local magnetic field vector at the 4 vertices. (b) An array of X-type magnetic field lines are shown obliquely aligned with the y axis when viewed from the x-direction. The magnitude of the magnetic fields on green and yellow surface are 16 nT and 2.5 nT, respectively. (c) A structure consisting of two convergent spines and a divergent fan is located adjacent to the tetrahedron when viewed from top. Magnetic fields on green and yellow surfaces are 26 nT and 1.5 nT, respectively.

and are plotted in Figure 1a. These data have an estimated accuracy of less than 0.1 nT. The "curlometer" [*Dunlop et al.*, 1988] linear estimate from Cluster measurements at 05:03:36 UT is 0.0268 nT/km. The curl of the fitted magnetic field at the Harris current neutral sheet is calculated to be 0.0331 nT/km at 05:03:36 UT. These two curl values are on the same order of magnitude.

[12] The plasma velocity measurements during the same interval with a 4 s resolution of the CIS on board Cluster [*Reme et al.*, 2001] are plotted in Figure 1b. Figures 1c, 1d, and 1e illustrate the reconstructed magnetic field configurations at 05:03:32, 05:03:36 and 05:03:39 UT, respectively, by using 1s-averaged magnetic field data, where magnetic field lines are indicated in black, the Cluster spacecraft positions are indicated by green rectangles, and the observed magnetic field direction in red arrows. We see an apparent X-point like magnetic field configuration at 05:03:36 UT, as shown in Figure 1d.

[13] At 05:03:32 UT, just before the reconnection event, the reconstructed field shows the magnetic field line bending tailward. After the reconnection event, at 05:03:39 UT, the field lines are found to bend earthward. This time sequence can be understood as the reconnection regions move earthward through the Cluster satellites. Such a temporal variation of the magnetic configuration is consistent with the observations of the negative-to-positive reversal of B_z and the positive-to-negative reversal of V_x during this interval as shown in Figures 1a and 1b, respectively.

[14] In Figure 1c, the magnetic field lines in the volume appear to be bending tailward and left part (earthward part) of the X-type field structure dominates the calculation volume at this moment. In Figure 1d, one can see the left part, central part, and right part of X-type field structure. In Figure 1e, right part (tailward part) of X-type field structure dominates the calculation volume. Therefore we can state that the reconnection site is moving earthwards through the Cluster satellites.

[15] No magnetic null exists in Figure 1c and Figure 1e respectively because the central part of X-type field structure where magnetic null may be located is outside or on the edge of the calculation volume at these two moments. We should point out that, the grey iso-B surfaces in Figures 1c–1e do not necessarily surround a magnetic null. If we decrease the B-value of these iso-B surfaces from 2.5 nT to 1.5 nT, then the iso-B surfaces in Figure 1c and Figure 1e disappear, which indicate that there is no magnetic null at 05:03:32 and 05:03:39 UT respectively.

[16] We now analyze in detail the reconstructed magnetic structure at 05:03:36 UT, and illustrate it from different viewing angles. Figure 2a shows a magnetic structure

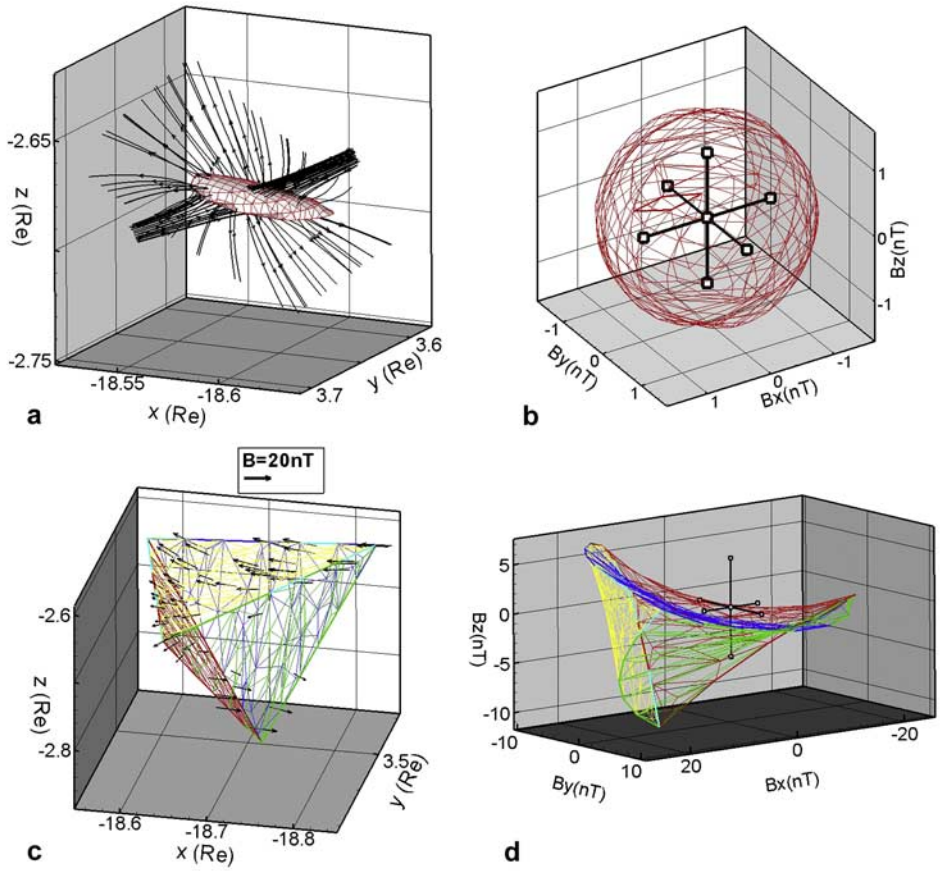

Figure 3. Mapping of magnetic field vectors from the configuration space (x, y, z) to the "M" space (B_x, B_y, B_z). (a) The magnetic field structure with two convergent spines and a divergent fan are placed in the GSM coordinate system with magnetic field lines denoted in black. The surface of B = 1.5 nT is marked by numerous positions scattered on it forming red meshes. (b) Mapping of magnetic field vectors in various positions on the red meshes in Figure 3a to the "M" space. Three black axes represent the "M" space coordinate system with the origin at B = 0 nT. (c) Four surfaces of the tetrahedron formed by Cluster constellation are partitioned into numerous meshes in red, green, blue and yellow respectively. Black arrows located at some nods of the meshes indicate some local magnetic field vectors. (d) The mapping of the tetrahedron in Figure 3c in the "M" space, with colors unchanged and the origin shown by the intersection of the three black bars.

appearing as an X-type configuration viewed in a diagonal direction in the x-y plane. It is found that such an X-type magnetic configuration is composed of an array of X-type magnetic field lines in a direction obliquely aligned to the y axis, as illustrated in Figure 2b. Figure 2c is the view from the direction looking down at the magnetic field configuration; it shows a typical 3-D magnetic null structure with a divergent fan and two convergent spines.

[17] The 3-D null point shown in Figure 2c can be further confirmed by using the field topological analysis. A null point in a small enough volume can be confirmed, if the origin of the coordinate system in "M" space (B_x, B_y, B_z) is located inside the closed "M" space surface which is mapped from a set of the magnetic field vectors on the closed space surface of this small volume [e.g., *Greene*, 1992; *Zhao et al.*, 2005]. Otherwise, no null point exists in the volume. Figure 3 demonstrates the use of the field topological analysis and confirms the existence of the null point. Figures 3a and 3b show that the iso-B surface with a small B-value in the reconstructed magnetic field does include a null point, whereas Figures 3c and 3d show that the null point is not located inside the Cluster tetrahedron. Figure 3a displays a closed iso-B surface with B = 1.5 nT. Magnetic field vectors at about 500 positions selected on that surface are then mapped to the "M" space, as illustrated in Figure 3b. The mapped surface is found to surround the origin in Figure 3b. Therefore the constructed magnetic structure here reconfirms the existence of a null point, which is presented in Figure 1 and Figure 2, in the vicinity of Cluster constellation at 05:03:36 UT. Figure 3c shows the magnetic vectors at about 400 positions on the tetrahedron surface of Cluster constellation. Finally, Figure 3d shows the closed surface in the "M" space mapped from those magnetic field vectors in Figure 3c. We see that the origin in "M" space is located outside of but close to the mapped surface. This result is consistent with the result shown in Figure 2c. The magnetic null identified outside the Cluster tetrahedron is reliable. We tested the fitting method pre-

sented in this paper with assumed 3-D elliptic flux tube structure, hyperbolic flux tube structure, and uniform field configuration. We found that the fitted field including a null geometry in the vicinity of the assumed tetrahedron is reliable.

[18] This null point belongs to the B-type category, since the eigenvalues for the gradient matrix of the magnetic field near the null, v_1, v_2, and v_3, are −0.0271, 0.0103, and 0.0168 (nT/km), respectively. Corresponding eigenvectors, $\vec{e}_1$, $\vec{e}_2$, and $\vec{e}_3$, are [0.9073, −0.0555, −0.4168], [−0.7814, −0.5013, −0.3716], and [0.6971, −0.5559, 0.4528], respectively. The latter two eigenvalues are real. This result shows no current flowing along the spine direction. However, this result should be considered as a result of the limitation of the fitting method which contains only a Harris current sheet.

4. Summary

[19] In this paper, a new method is presented for the first time to identify a magnetic structure around a magnetic null in the magnetotail using Cluster observations. The method is developed for reconstructing the local magnetic field based on the Cluster four satellite measurements by making use of a fitting function approach with 10 fitting parameters in 10 spherical harmonic functions and another two fitting parameters in the Harris current sheet model, thus matching the 12 observed field components. With this method we have reconstructed the local magnetic field by fitting the magnetic field vectors measured simultaneously by the four satellites of Cluster. With this fitted magnetic field we calculate the Poincaré index with a closed surface very near to the null. Magnetic field vectors at about 500 positions on the closed surface are selected for this calculation. The calculations confirm the existence of a magnetic field null. With the fitted results we present from in situ observations, a magnetic structure around a 3-D null in the magnetotail.

[20] In general it is necessary to make assumptions for reconstructing magnetic field with limited observation data. In the method presented here we assume a potential field plus a Harris current sheet field. We also examine this fitting method by reconstructing assumed typical model fields, such as the elliptic flux tube and the hyperbolic flux tube structures, and find consistent fitting results. Therefore the assumption and the fitting method are applicable for the geo-magnetotail.

[21] **Acknowledgments.** This work is supported by the National Natural Science Foundation of China under contracts 40574078, 40336053 and 40436015, the foundation Major Project of National Basic Research under contract 2006CB806305, as well as the Beijing Education Project XK100010404.

[22] Amitava Bhattacharjee thanks C E Parnell and John Finn for their assistance in evaluating this paper.

References

Aulanier, G., et al. (2000), The topology and evolution of the Bastille day flare, *Astrophys. J.*, *540*, 1126–1146.

Balogh, A., et al. (1997), *The Cluster and Phoenix Missions*, edited by C. P. Escoubet et al., pp. 65–92, Kluwer Academic, Dordrecht.

Birn, J., and E. R. Priest (Eds.) (2007), *Reconnection of Magnetic Fields*, Cambridge Univ. Press, Cambridge.

Birn, J., et al. (2001), Geospace Environment Modelling (GEM) magnetic reconnection challenge, *J. Geophys. Res.*, *106*, 3715.

Büchner, J. (1999), Three-dimensional magnetic reconnection in astrophysical plasmas-kinetic approach, *Astrophys. Space Sci.*, *264*, 25–42.

Deng, X. H., and H. Matsumoto (2001), Rapid magnetic reconnection in the Earth's magnetosphere generated by whistler waves, *Nature*, *410*, 557–559.

Ding, W. X., et al. (2004), Measurement of the Hall Dynamo Effect during magnetic reconnection in a high-temperature plasma, *Phys. Rev. Lett.*, *93*, doi:10.1103/PhysRevLett.93.045002.

Dorelli, J. C., A. Bhattacharjee, and J. Raeder (2007), Separator reconnection at Earth's dayside magnetopause under generic northward interplanetary magnetic field conditions, *J. Geophys. Res.*, *112*, A02202, doi:10.1029/2006JA011877.

Dunlop, M. W., D. J. Southwood, K. H. Glassmeier, and F. M. Neubauer (1988), Analysis of multipoint magnetometer data, *Adv. Space Res.*, *8*(9–10), (9)273–(9)277.

Escoubet, C. P., R. Schmidt, and M. L. Goldstein (1997), *The Cluster and Phoenix Missions*, edited by C. P. Escoubet et al., pp. 11–32, Kluwer Academic, Dordrecht.

Filippov, B. (1999), Observation of a 3D magnetic null point in the solar corona, *Sol. Phys.*, *185*, 297–309.

Fletcher, L., et al. (2001), Evidence for the flare trigger site and three-dimensional reconnection in multiwavelength observations of a solar flare, *Astrophys. J.*, *554*, 451–463.

Frey, H. U., T. D. Phan, S. A. Fuselier, and S. B. Mende (2003), Continuous magnetic reconnection at Earth's magnetopause, *Nature*, *426*, 533–536.

Greene, J. M. (1988), Geometrical properties of 3 D reconnecting magnetic fields with nulls, *J. Geophys. Res.*, *93*, 8583–8590.

Greene, J. M. (1992), Locating three-dimensional roots by a bisect ion method, *J. Comput. Phys.*, *98*, 194–198.

Harris, M. J. (1962), On a plasma sheet separating regions of oppositely directed magnetic field, *Nuovo Cimento*, *23*, 115–121.

Henderson, P. D., et al. (2006), Cluster PEACE observations of electron pressure tensor divergence in the magnetotail, *Geophys. Res. Lett.*, *33*, L22106, doi:10.1029/2006GL027868.

Lin, J., et al. (2005), Direct observations of the magnetic reconnection site of an eruption on 2003 November 18, *Astrophys. J.*, *622*, 1251–1264.

Nagai, T., et al. (2001), Geotail observations of the Hall current system: Evidence of magnetic reconnection in the magnetotail, *J. Geophys. Res.*, *106*, 25929.

Øieroset, M., et al. (2001), In situ detection of collisionless reconnection in the earth's magnetotail, *Nature*, *412*, 414–417.

Parker, E. N. (1957), Sweet's mechanism for merging magnetic fields in conducting fluids, *J. Geophys. Res.*, *62*, 509.

Parnell, C. E., J. Smith, T. Neukirch, and E. R. Priest (1996), The structure of three-dimensional magnetic neutral points, *Phys. Plasmas*, *3*, 759–770.

Petschek, H. E. (1964), Magnetic field annihilation, in *AAS-NASA Symposium on the Physics of Solar Flares*, NASA Spec. Publ. 5P-50, 425.

Phan, T. D., et al. (2000), Extended magnetic reconnection at the earth's magnetopause from detection of bi-directional jets, *Nature*, *404*, 848–850.

Priest, E. R., and P. Demoulin (1995), Three-dimensional reconnection without null points, *J. Geophys. Res.*, *100*, 23,443–23,463.

Priest, E. R., and T. G. Forbes (1989), Steady magnetic reconnection in three dimensions, *Sol. Phys.*, *119*, 211–214.

Priest, E. R., and T. G. Forbes (2000), *Magnetic Reconnection: MHD Theory and Applications*, Cambridge Univ. Press, New York.

Priest, E. R., and V. S. Titov (1996), Magnetic Reconnection At Three-Dimensional Null Points, *Philos. Trans. R. Soc. Ser. A And Ser. B*, *A 354*, 2951–2992.

Pritchett, P. L., and F. V. Coroniti (2004), Three-dimensional collisionless magnetic reconnection in the presence of a guide field, *J. Geophys. Res.*, *109*, A01220, doi:10.1029/2003JA009999.

Reme, H., et al. (2001), First multispacecraft ion measurements in and near the Earth's magnetosphere with the identical Cluster Ion Spectrometry (CIS) experiment, *Ann. Geophys.*, *19*, 1303–1354.

Ricci, P., et al. (2004), Collisionless magnetic reconnection in the presence of a guide field, *Phys. Plasmas*, *11*(8), 4102, doi:10.1063/1.1768552.

Sweet, P. A. (1958), The neutral point theory of solar flare, in *Electromagnetic Phenomena in Cosmical Physics*, edited by B. Lehnert, Cambridge Univ. Press, London.

Vaivads, A., et al. (2004), Cluster observations of lower hybrid turbulence within thin layers at the magnetopause, *Geophys. Res. Lett.*, *31*, L03804, doi:10.1029/2003GL018142.

Xiao, C. J., et al. (2006), In situ evidence for the structure of the magnetic null in a 3D reconnection event in the Earth's magnetotail, *Nature Phys.*, *2*, 478–483, doi:10.1038/nphys342.

Xiao, C. J., et al. (2007), A Cluster measurement of fast magnetic reconnection in the magnetotail, *Geophys. Res. Lett.*, *34*, L01101, doi:10.1029/2006GL028006.

Zhao, H., J. Wang, J. Zhang, and C. J. Xiao (2005), A new method of identifying 3D null points in solar vector magnetic fields, *Chin. J. Astron. Astrophys.*, *5*, 443–447.

I. Dandouras and H. Reme, Centre d'Etude Spatiale des Rayonnements, BP 4346, 31028 Toulouse Cedex 4, France.

M. W. Dunlop, Space Sciences Division, SSTD, Rutherford Appleton Laboratory, Chilton, Oxfordshire OX1100X, UK.

C. P. Escoubet, ESA/ESTEC, Postbus 299, 220 AG Noordwijk, Netherlands.

S.-Y. Fu, J.-S. He, Z.-Y. Pu, H. Tian, and Q.-G. Zong, School of Earth and Space Sciences, Peking University, Beijing 100871, China.

K.-H. Glassmeier, IGEP, Technische Universität Braunschweig, Braunschweig, Germany.

Z.-X. Liu, CSSAR, Chinese Academy of Sciences, Beijing 100080, China.

Z.-W. Ma, Institute for Fusion Theory and Simulation, Zhejiang University, Hangzhou 310027, China.

C.-Y. Tu, Department of Geophysics, Peking University, Beijing 100871, China. (chanyitu@pku.edu.cn)

J.-X. Wang, C.-J. Xiao, H. Zhao, and G.-P. Zhou, National Astronomical Observatories, Chinese Academy of Sciences, Beijing 10012, China.

X.-G. Wang, School of Physics, Peking University, Beijing 100871, China.